HHS Public Access

Author manuscript

Ultrason Imaging. Author manuscript; available in PMC 2016 January 01.

Published in final edited form as:

Ultrason Imaging. 2016 January ; 38(1): 44–62. doi:10.1177/0161734615584312.

Multi-scale Functional and Molecular Photoacoustic Tomography

Junjie Yao[1], **Jun Xia**[1,2], and **Lihong V. Wang**[1,*]

[1]Optical Imaging Laboratory, Department of Biomedical Engineering, Washington University in St. Louis, MO 63130

[2]Department of Biomedical Engineering, University at Buffalo, The State University of New York, Buffalo, NY 14260

Abstract

Photoacoustic tomography (PAT) combines rich optical absorption contrast with the high spatial resolution of ultrasound at depths in tissue. The high scalability of PAT has enabled anatomical imaging of biological structures ranging from organelles to organs. The inherent functional and molecular imaging capabilities of PAT have further allowed it to measure important physiological parameters and track critical cellular activities. Integration of PAT with other imaging technologies provides complementary capabilities and can potentially accelerate the clinical translation of PAT.

Keywords

photoacoustic tomography; photoacoustic microscopy; photoacoustic computed tomography; multi-scale imaging; functional imaging; molecular imaging

Introduction

Photoacoustic (PA, also termed optoacoustic) tomography (PAT) is a hybrid imaging modality that acoustically detects the optical absorption contrast of biological tissue [1–4]. In PAT, the object is usually irradiated by a short-pulsed laser beam. Some of the incident photons are absorbed by biomolecules (e.g., hemoglobin, water, lipids and melanin), and their energy is partially or completely converted into heat. The heat-induced pressure propagates in tissue as wideband ultrasound waves, which are detected outside the tissue by an ultrasonic transducer or transducer array to form an image that maps the original optical energy deposition in the tissue [5].

PAT seamlessly combines the rich optical absorption contrast of biological tissue with the high acoustic resolution at depths. In the optical excitation phase, a given percentage change in the optical absorption coefficient of the tissue yields the same percentage change in the linear PA signal amplitude; hence PAT has 100% sensitivity to optical absorption contrast. In the acoustic detection phase, the ultrasound waves undergo only weak scattering in tissue,

*Corresponding author: lhwang@wustl.edu.

which enables high-resolution PA imaging at depths beyond the optical diffusion limit (~1 mm in tissue) [6].

Benefiting from fast advances in laser and ultrasound technologies, PAT has developed remarkably since the early 2000s [7–9]. Almost all the key performance aspects of PAT, including spatial resolution, penetration depth, imaging speed and detection sensitivity, have been continuously improved through collaborative efforts involving engineering, mathematics, materials science, chemistry and biomedicine. Building on these technical advances, PAT has become increasingly popular in preclinical studies, especially in studying tumor angiogenesis, cancer hypoxia, brain functions, tissue remodeling and drug delivery [1, 2]. Most encouragingly, PAT has started to be used in clinical practice, for procedures such as breast cancer screening [10–12], sentinel lymph node mapping [13–18], melanoma staging [19–24] and endoscopic examination [25, 26]. All of these preclinical and clinical applications of PAT are important maturing steps towards human healthcare.

In light of the deep connections between PAT and ultrasound imaging [5, 27], this concise Review aims to introduce PAT technologies to the general ultrasound community, highlighting its inherent functional and molecular imaging capabilities. Representative PAT applications in both fundamental studies and clinical practice will be reviewed. Integration of PAT with other imaging modalities will also be discussed, and finally, potential PAT technical breakthroughs will be envisioned.

Multi-scale PAT: seeing clearly at depths

Photon propagation in soft tissue can be loosely classified into four regimes, which are approximately related to the penetration depths of representative optical imaging modalities (Figure 1a) [5, 28]. Conventional planar optical microscopy works within the aberration limit (~100 μm, ballistic regime), where photons have undergone no scattering [5]. Modern optical imaging modalities, such as confocal microscopy, two-photon microscopy and optical coherence tomography, are limited by diffusion to ~1 mm in soft tissue (quasi-ballistic regime), where scattered photons still retain strong memory of original propagation direction [4]. Diffuse optical tomography (DOT) and PAT are able to provide penetration into the quasi-diffusive and diffusive regimes where photons have almost completely lost their memory of the original propagation direction [5, 29, 30]. However, DOT and PAT are still limited by dissipation to less than 10 cm in soft tissue, where the optical fluence (J/m^2) is significantly attenuated due to both absorption and scattering. Finally, when the optical scattering is largely corrected for by using wavefront engineering technologies, it is believed to be possible to conquer the dissipation limit and approach the absorption limit (~1 m) for whole-body penetration in humans [31, 32]. For brevity, the following use of “diffusive” and “ballistic” in this Review also refers to “quasi-diffusive” and “quasi-ballistic”, respectively.

In contrast, ultrasound attenuation in soft tissue is dominated by absorption instead of scattering [33, 34]. For example, at 5 MHz, the ultrasound scattering coefficient of the human skin is 0.014 cm^{-1} while the ultrasound attenuation coefficient is 0.38 cm^{-1}. The ultrasound attenuation coefficient is approximately proportional to the ultrasound frequency

over a wide frequency range [34–36]. In fact, a good rule of thumb is that the ultrasound attenuation coefficient for a variety of soft tissues is 0.5–1.0 dB/cm/MHz [34]. Such frequency-dependent attenuation in ultrasound imaging results in the trade-off between its spatial resolution and penetration depth. Figure 1b shows the approximate ultrasound penetration depths at typical frequencies and the corresponding biomedical applications.

Since PAT utilizes optical excitation and acoustic detection, its resolution can be either optically or acoustically determined, depending on the targeted penetration depth. Classified by how its resolution is determined, PAT has two major implementations [1]: acoustic-resolution PAT with an imaging depth beyond the optical diffusion limit; and optical-resolution PAT with an imaging depth less than the optical diffusion limit. Readers are referred to recent Review articles for comprehensive details about different PAT implementations [3, 37–39].

Acoustic-resolution PAT

Acoustic-resolution PAT targets deep tissue imaging with acoustically determined resolutions in all dimensions. Acoustic-resolution PAT can be implemented by raster-scanning weakly focused optical illumination and a spherically focused ultrasonic transducer, a technology typically referred to as acoustic-resolution photoacoustic microscopy (AR-PAM). Acoustic-resolution PAT can also be implemented by using wide-field optical illumination and parallel acoustic detection with an ultrasonic transducer array, a technology typically referred to as photoacoustic computed tomography (PACT). In acoustic-resolution PAT, both the spatial resolution and imaging depth are highly scalable with the ultrasound frequency. PAT operating with lower ultrasound frequency can penetrate deeper with relaxed resolution.

As a rule of thumb, different acoustic-resolution PAT embodiments have generally achieved a depth-to-resolution ratio (DRR) of ~200 [1]. For example, by using a 50 MHz focused ultrasonic transducer, the first AR-PAM achieved a lateral resolution of ~45 μm, an axial resolution of ~15 μm and an imaging depth of ~3 mm in tissue [8, 40]. Such an imaging depth is sufficient for melanoma staging [40] and pain treatment evaluation [41] in the human skin. By using a similar design but with a 5 MHz transducer, photoacoustic macroscopy (PAMac) increased the imaging depth to ~38 mm, with a relaxed lateral resolution of ~500 μm and axial resolution of ~144 μm [42, 43]. This imaging depth is sufficient for whole-body mouse imaging (Figure 2a) [43] and deep sentinel lymph node mapping [13–18].

Acoustic-resolution PAT has proven powerful in deep tissue imaging, such as human breast cancer detection [11–13, 44–46], prostate adenocarcinoma imaging [47, 48], atherosclerotic plaque characterization [26], ophthalmic imaging [49], gastrointestinal (GI) tract imaging [50], small animal whole-body imaging [51–53] and thyroid imaging [54]. Of all the clinical translations of PAT, human breast imaging has progressed furthest. So far, several groups have reported PA breast imaging on a total of more than 100 patients [37]. To accommodate the shape of the uncompressed breast, Kruger and his colleagues used a semi-spherical transducer array with rotational scanning for dense spatial sampling (Figure 2b) [12].

However, this configuration suffers from low imaging speed and may have difficulty in detecting deep tumors. Kitai and his colleagues used a 2D planar transducer array, where the breast was gently compressed from the side between a glass slide and the transducer array [45]. The side compression can reduce the effective beast thickness and thus help detect deeper tumors. However, the planar detection geometry suffers from limited view for accurate reconstruction. Alternatively, our laboratory has developed an integrated PAT and thermoacoustic tomography (TAT) system, where the breast is compressed from the front (the nipple side) to form a cylindrical shape [55]. The illumination is directed from the front, and the ultrasonic transducers scan around and along the cylindrical breast to obtain a full 3D data set. In this configuration, deep tumors close to the chest wall can potentially be imaged.

Optical-resolution PAT

Although acoustically determined resolutions in acoustic-resolution PAT are adequate for many biomedical applications, it becomes challenging to improve the spatial resolutions to the cellular level by simply increasing the ultrasound frequency without severely compromising the penetration [34, 56, 57]. Different from ultrasound imaging, PAT can use fine optical focusing to provide optically defined lateral resolution within the optical diffusion limit, while the axial resolution is still derived from the time-resolved ultrasonic detection.

Optical-resolution PAT is traditionally referred to as optical-resolution photoacoustic microscopy (OR-PAM) [52, 58–74]. Limited only by optical diffraction, the lateral resolution of OR-PAM can easily reach the cellular and subcellular level, and is scalable with the optical wavelength and the numerical aperture (NA) of the optical objective. The first OR-PAM, reported in 2008, achieved a lateral resolution of ~5 μm (objective NA: 0.1 in air) and an imaging depth of ~1 mm. Single capillaries in a mouse ear can be clearly resolved (Figure 2c) [64]. The lateral resolution of OR-PAM was later improved to ~220 nm by using a water-immersion objective (objective NA: 1.23 in water), allowing single red blood cells to be clearly resolved (Figure 2d) [75]. Further, in recently developed optical-resolution PACT systems, the field of view is simultaneously excited by an array of diffraction-limited optical foci, and the resultant PA waves are detected by a linear- or ring-shape ultrasonic transducer array [69, 76, 77]. The parallel excitation and detection enable fast wide-field imaging, while the imaging depth is still restricted to ~1 mm.

Recently, OR-PAM has succeeded in sub-optical-diffraction imaging, taking advantage of various nonlinear mechanisms such as two-photon absorption [78–80], photobleaching [81], absorption saturation [82] and thermal relaxation [82, 83]. Nonlinear OR-PAM has provided optically determined resolutions in all dimensions including the axial or depth direction. In particular, a sub-diffraction lateral resolution of ~80 nm has been achieved by photoacoustic nanoscopy using the absorption saturation effect, enabling single mitochondria in fibroblast cells to be resolved (Figure 2e) [82]. Meanwhile, an axial resolution on the level of sub-micrometers has been achieved, which is about two orders of magnitude finer than the acoustically determined axial resolution in traditional linear OR-PAM [81, 82].

Functional and molecular PAT: seeing more than anatomy

While functional ultrasound imaging is largely limited to Doppler ultrasound and molecular ultrasound imaging mostly detects microbubbles in the vasculature [27], PAT is inherently suited for diverse functional and molecular imaging, with a wealth of endogenous and exogenous contrasts.

Functional PAT

So far, PAT has measured a number of functional parameters at various length scales, including total hemoglobin concentration [12, 63, 84–86], blood oxygenation [85–92], temperature [93–95], blood flow [96–102], pH [103–106], blood glucose level [107], pulse-wave velocity [108] and metabolic rate of oxygen (MRO_2) [22, 109, 110]. Here we discuss several widely measured functional parameters, especially for cancer diagnosis and therapy.

Hemoglobin in red blood cells carries most of the oxygen needed by the body to power its functions [111]. Using hemoglobin as the endogenous contrast, PAT can quantify the total hemoglobin concentration (HbT) and oxygen saturation of hemoglobin (sO_2) with high sensitivity (Figures 3a–b) [112]. For accurate measurement of absolute HbT and sO_2, it is necessary to correct for light attenuation by using empirical or model-based methods [89–91, 113–116]. Recently, single-wavelength-based and dynamics-based PA methods have also been developed for absolute sO_2 measurement [88, 117]. Notably, HbT and sO_2 measurements are proven useful in cancer diagnosis and prognosis. For example, in PA breast cancer imaging, increased HbT in the tumor region is highly correlated with cancer angiogenesis (Figure 3c) [45], while decreased sO_2 in the tumor core typically indicates an adverse cancer progression [118, 119].

During thermotherapy, it is necessary to monitor the local temperature for safe deposition of heat and efficient destruction of abnormal cells. Using the temperature dependence of the Grueneisen parameter [120–127], PAT can measure temperature changes from relative changes in PA amplitude alone [93, 128]. A temperature detection sensitivity of 0.15 °C was achieved with a temporal resolution of 2 seconds [93]. Furthermore, a recently published method can quantify the absolute temperature in deep tissue with AR-PAM and PACT, using the dual temperature dependences of the Grueneisen parameter and the speed of sound [129, 130]. In addition to measuring temperature, the temperature dependence of PA signal can also be used to measure the blood flow speed in deep tissue [101, 131], enhance the spatial resolution of OR-PAM [82] and ameliorate the limited-view problem in linear-array-based PACT [131].

Blood flow ensures the transportation of oxygen, nutrients and metabolic wastes throughout the body. PAT can measure blood flow by using either Doppler methods [97, 99, 102, 132–135] or feature-tracking methods [98, 100, 101, 136, 137]. Compared with ultrasound flowmetry, PA flowmetry has much higher detection sensitivity because of the excellent contrast between the blood vessels and the surrounding tissue. A flow detection sensitivity of 50 μm/s has been demonstrated by using a structured-illumination PA method [135]. In addition, thermal-tagging methods have measured flow speeds at 5 mm depth in tissue [100, 101, 136, 137]. Consequently, by simultaneously measuring multiple parameters such as

HbT, sO_2 and blood flow, PAT can quantify the metabolic rate of oxygen (MRO_2) of tissue, which can potentially be used for early cancer detection [22, 109, 110].

Molecular PAT

In addition to functional imaging, by using targeted or untargeted contrast agents, PAT can track molecular processes in living organisms [21, 138–145]. The choice of contrast agents for molecular PAT is much greater than for molecular ultrasound imaging, because all molecules have their own absorption wavelengths, hence they can be imaged by PAT [38, 39]. In addition, many molecules can reach the extravascular space. So far, many contrast agents have been imaged in molecular PAT [37, 38, 146], including organic dyes (Figure 4a), nanoparticles (Figure 4b), fluorescent proteins (Figure 4c), microbubbles and reporter gene products (Figure 4d). These contrast agents, especially nanoparticles [141], can be specifically engineered for different PA applications.

The detection sensitivity of molecular PAT is relevant to a number of factors, such as the absorption cross-section of the molecule, the sensitivity of the ultrasonic transducer, the imaging depth and the permitted light exposure [147]. Roughly, in molecular PAT, the reported noise-equivalent detectable concentration at ≥3 mm depth in tissue is on the level of millimolar for microbubbles, micromolar for organic dyes, nanomolar for proteins and picomolar for nanoparticles [44, 148–153].

Molecular PAT has been proven reliable in early cancer imaging, circulating tumor cell (CTC) detection, glucose uptake monitoring and sentinel lymph node mapping (Figure 3e) [151, 154, 155]. For example, PAT has been successfully used for detecting pigmented circulating melanoma cells, due to their strong light absorption [21, 156, 157]. Recently, non-pigmented circulating breast cancer cells have also been detected *in vivo* by PAT, using targeted gold nanoparticles [158] or genetically-encoded green fluorescent protein [159] as the contrast agent. Multi-spectral PA measurements can help unmix different molecules to enhance the detection of CTCs [142] and early-stage tumors [160]. Magnetically modulated PA detection can highlight the signals from magnetic nanoparticles targeted to tumor cells [142]. Activatable organic dyes and nanoparticles can also help detect cellular activities of interest, with improved sensitivity (Figure 3f) [54, 156].

It is worth noting that multi-wavelength illumination is often required in functional and molecular PA imaging. However, commercially available wavelength-tunable lasers (e.g., dye lasers, optical parametric oscillators, or Ti:sapphire lasers) cannot switch wavelengths at a high speed [161]. Several methods have been developed to achieve fast wavelength tuning. Dean-Ben and his colleagues customized a 50 Hz optical parametric oscillator that allowed wavelength change on a per-pulse basis for their hemi-spherical-array-based PACT [162]. Wang et al. have developed a digital-mirror-device based wavelength multiplexing method for OR-PAM with a wideband dye laser [163]. A 2 kHz wavelength tuning speed has been achieved with a wavelength tunable range of ~20 nm. In addition, two lasers with different wavelengths can serve as an alternative to wavelength tuning, with increased system cost [164].

Integration of PAT with other imaging modalities

A major challenge for quantitative PAT is the unknown local light fluence. This issue can potentially be addressed by integrating PAT with DOT, which measures the optical properties of the tissue. Multiple groups have reported various DOT-PAT systems for different applications [165–168]. Studies have shown that DOT allows better quantitative reconstruction in PAT [165, 167, 169]. However, the optical properties derived from DOT measurements typically possess much poorer spatial resolution than that of PAT. Iterating between PAT and DOT reconstructions may help resolve this issue [167].

Speed of sound (SOS) heterogeneities also deteriorate PAT image quality. One remedy is to combine PAT with ultrasound tomography (UST). In UST-PAT systems, UST provides the SOS map of the tissue to improve the PAT reconstruction. Unlike the combination of PAT with DOT, which requires additional light sources and detectors, the addition of UST to PAT can be implemented with existing ultrasonic transducers as long as the ultrasonic transmission capability is enabled [170]. Alternatively, PAT can be integrated with commercial UST by adding a pulsed light source [13]. In addition to heterogeneous SOS, acoustic attenuation and aberration also deteriorate PAT image quality [170–173], especially in human brain PAT; but their effects can be potentially investigated with UST-PAT as well.

In addition to correcting for optical and acoustic inhomogeneities, different PAT embodiments have also been integrated with other imaging modalities to provide complementary contrasts [174]. Deep-penetration imaging modalities, such as magnetic resonance imaging (MRI), X-ray computed tomography (CT) and positron emission tomography (PET), have been used in conjunction with PAT for studies involving multimodality contrast agents [175–177]. PAT has been integrated with confocal microscopy [178, 179], optical coherence tomography [180–183] and ultrasound imaging [13, 18, 26, 50, 184–186], sharing either the same optical components or ultrasonic transducer(s) (Figure 5a) [50]. A recently developed tri-modality optical imaging system combines OR-PAM with a commercial confocal and two-photon microscopic system (Figure 5b) [187]. The three imaging modalities can readily share the optical illumination path and scanning system.

Discussion

In conclusion, PAT is a unique imaging modality that complements other imaging techniques: rich optical absorption contrast provides inherent functional and molecular imaging capabilities, and acoustic detection allows high resolution imaging at depths. Although we can cover only several representative studies in this concise Review, they have clearly showed the scale and momentum of PAT development. Here, we will also discuss a few potential breakthroughs of PAT technologies.

One new frontier is PA-based optical wavefront engineering. The ability to focus light deep into tissue will have tremendous impacts on imaging and therapy. By using PA signals as the feedback, the wavefront of the excitation light can be optimized through iterative algorithms so that it can be confined to either an acoustically or optically determined region

in the tissue [188, 189]. The advantage of PA detection is its high resolution and deep penetration, while the slow optimization process remains to be a major challenge.

Miniaturizing the PA probe is essential for endoscopic and intravascular applications. Recently, several PA endoscopes have been developed with optical detection of the acoustic signals [190–193]. Since the detection sensitivity of these optical detectors (e.g., micro-ring resonators and Fabry-Perot sensors) is not directly related to the detector size, the PA probe size can be significantly reduced. However, none of those optical detectors have been used for acoustic-resolution endoscopic imaging in deep tissue, due to the lack of acoustic focusing capability. Alternatively, internal optical illumination through the body cavity can be combined with external acoustic detection [194], avoiding the problem of acoustic detector size.

There is also great interest in hand-held PA probes for imaging surface regions such as the face, neck and arm, which are difficult to access with traditional table-top PAT systems. Several hand-held PA probes have been developed for microvascular imaging of port-wine stains on the face [195, 196], blood oxygenation imaging of the jugular vein in the neck [197], sentinel lymph node mapping in the breast [198], and melanoma imaging on the skin [199, 200]. For these hand-held PA probes, the imaging speed still needs to be improved to mitigate motion artifacts from both the patient and operator.

Although PAT is relatively inexpensive compared with MRI and PET, further reducing its cost can accelerate clinical translation. The most expensive components in PAT are typically the pulsed laser source and the ultrasonic transducer array. Several groups have explored inexpensive light sources [183, 201–205]. For example, Li et al. have developed an OR-PAM system using a low-cost Blue-ray DVD pickup head with a 405 nm laser diode [205]. An inexpensive ultrasound detector is also of interest, because the ultrasound receiving system becomes significantly more costly as the number of transducer elements increases. A PAT system based on low-cost acoustic delay lines for acoustic detection has been reported [206, 207]. Nevertheless, the acoustic coupling efficiency and the number of the acoustic delay lines still need to be increased.

At last, with its nonionizing radiation, high image quality, and functional and molecular imaging capabilities, PAT holds great promise for disease detection, staging and treatment evaluation. Although many challenges remain, none of them are beyond reach. PA breast cancer screening is now most ready for clinical translation. PA endoscopic examination of the GI tract will provide functional information at unprecedented depths. PA melanoma detection at depths up to a few millimeters will significantly improve the cancer’s staging accuracy. Finally, PA human brain imaging through intact scalp and skull, although technically challenging, is considered one of the most promising tools for functional brain studies, with breakthroughs expected soon.

Acknowledgments

The authors appreciate Prof. James Ballard’s close reading of the manuscript. This work was sponsored in part by NIH grants DP1 EB016986 (NIH Director’s Pioneer Award), R01 CA186567 (NIH Director’s Transformative Research Award), U01 NS090579 (BRAIN Initiative). L. V. Wang has a financial interest in Endra, Inc., and Microphotoacoustics, Inc., which, however, did not support this work.

References

1. Wang LHV, Hu S. Photoacoustic Tomography: In Vivo Imaging from Organelles to Organs. Science. 2012; 335(6075):1458–1462. [PubMed: 22442475]
2. Wang LV. Multiscale photoacoustic microscopy and computed tomography. Nature Photonics. 2009; 3(9):503–509. [PubMed: 20161535]
3. Beard P. Biomedical photoacoustic imaging. Interface Focus. 2011; 1(4):602–631. [PubMed: 22866233]
4. Ntziachristos V. Going deeper than microscopy: the optical imaging frontier in biology. Nature Methods. 2010; 7(8):603–614. [PubMed: 20676081]
5. Wang, LV.; Wu, H-i. Biomedical optics : principles and imaging. Vol. xiv. Hoboken, N.J: Wiley-Interscience; 2007. p. 362
6. Yao J, Wang LV. Photoacoustic tomography: fundamentals, advances and prospects. Contrast Media Mol Imaging. 2011; 6(5):332–345. [PubMed: 22025335]
7. Wang XD, Pang YJ, Ku G, Xie XY, Stoica G, Wang LHV. Noninvasive laser-induced photoacoustic tomography for structural and functional in vivo imaging of the brain. Nature Biotechnology. 2003; 21(7):803–806.
8. Zhang HF, Maslov K, Stoica G, Wang LHV. Functional photoacoustic microscopy for high-resolution and noninvasive in vivo imaging. Nature Biotechnology. 2006; 24(7):848–851.
9. Andreev VG, Karabutov AA, Oraevsky AA. Detection of ultrawide-band ultrasound pulses in optoacoustic tomography. IEEE transactions on ultrasonics, ferroelectrics, and frequency control. 2003; 50(10):1383–90.
10. Eghtedari M, Copland JA, Kotov NA, Oraevsky AA, Motamedi M. Optoacoustic imaging of nanoparticle labeled breast cancer cells: A molecular based approach for imaging of deep tumors. Lasers in Surgery and Medicine. 2004; S16:52–52.
11. Frangioni JV. New technologies for human cancer imaging. Journal of Clinical Oncology. 2008; 26(24):4012–4021. [PubMed: 18711192]
12. Kruger RA, Lam RB, Reinecke DR, Del Rio SP, Doyle RP. Photoacoustic angiography of the breast. Medical Physics. 2010; 37(11):6096–6100. [PubMed: 21158321]
13. Kim C, Erpelding TN, Jankovic L, Pashley MD, Wang LHV. Deeply penetrating in vivo photoacoustic imaging using a clinical ultrasound array system. Biomedical Optics Express. 2010; 1(1):278–284. [PubMed: 21258465]
14. Pan DPJ, Cai X, Yalaz C, Senpan A, Omanakuttan K, Wickline SA, et al. Photoacoustic Sentinel Lymph Node Imaging with Self-Assembled Copper Neodecanoate Nanoparticles. Acs Nano. 2012; 6(2):1260–1267. [PubMed: 22229462]
15. Pan DPJ, Pramanik M, Senpan A, Ghosh S, Wickline SA, Wang LV, et al. Near infrared photoacoustic detection of sentinel lymph nodes with gold nanobeacons. Biomaterials. 2010; 31(14):4088–4093. [PubMed: 20172607]
16. Song KH, Kim CH, Cobley CM, Xia YN, Wang LV. Near-Infrared Gold Nanocages as a New Class of Tracers for Photoacoustic Sentinel Lymph Node Mapping on a Rat Model. Nano Letters. 2009; 9(1):183–188. [PubMed: 19072058]
17. Song KH, Stein EW, Margenthaler JA, Wang LV. Noninvasive photoacoustic identification of sentinel lymph nodes containing methylene blue in vivo in a rat model. Journal of Biomedical Optics. 2008; 13(5):054033. [PubMed: 19021413]
18. Wang Y, Erpelding TN, Jankovic L, Guo ZJ, Robert JL, David G, et al. In vivo three-dimensional photoacoustic imaging based on a clinical matrix array ultrasound probe. Journal of Biomedical Optics. 2012; 17(6):061208. [PubMed: 22734738]
19. Staley J, Grogan P, Samadi AK, Cui H, Cohen MS, Yang X. Growth of melanoma brain tumors monitored by photoacoustic microscopy. Journal of Biomedical Optics. 2010; 15(4):040510. [PubMed: 20799777]
20. Kim C, Cho EC, Chen JY, Song KH, Au L, Favazza C, et al. In Vivo Molecular Photoacoustic Tomography of Melanomas Targeted by Bioconjugated Gold Nanocages. Acs Nano. 2010; 4(8): 4559–4564. [PubMed: 20731439]

21. Galanzha EI, Shashkov EV, Spring PM, Suen JY, Zharov VP. In vivo, Noninvasive, Label-Free Detection and Eradication of Circulating Metastatic Melanoma Cells Using Two-Color Photoacoustic Flow Cytometry with a Diode Laser. Cancer Research. 2009; 69(20):7926–7934. [PubMed: 19826056]
22. Yao J, Maslov KI, Zhang Y, Xia Y, Wang LV. Label-free oxygen-metabolic photoacoustic microscopy in vivo. Journal of Biomedical Optics. 2011; 16(7):076003. [PubMed: 21806264]
23. Cheng Z, Levi J, Xiong ZM, Gheysens O, Keren S, Chen XY, et al. Near-infrared fluorescent deoxyglucose analogue for tumor optical imaging in cell culture and living mice. Bioconjugate Chemistry. 2006; 17(3):662–669. [PubMed: 16704203]
24. Qin CX, Cheng K, Chen K, Hu X, Liu Y, Lan XL, et al. Tyrosinase as a multifunctional reporter gene for Photoacoustic/MRI/PET triple modality molecular imaging. Scientific Reports. 2013; 3:1490. [PubMed: 23508226]
25. Yang, J-M.; Chen, R.; Favazza, C.; Yao, J.; Zhou, Q.; Shung, KK., et al. Photons Plus Ultrasound: Imaging and Sensing 2012. San Francisco, California, USA: SPIE; 2012. A 2.5-mm outer diameter photoacoustic endoscopic mini-probe based on a highly sensitive PMN-PT ultrasonic transducer; p. 82233M-6
26. Wang B, Su JL, Karpiouk AB, Sokolov KV, Smalling RW, Emelianov SY. Intravascular Photoacoustic Imaging. Ieee Journal of Selected Topics in Quantum Electronics. 2010; 16(3):588–599.
27. Cobbold, RSC. Foundations of biomedical ultrasound. Vol. xix. Oxford ; New York: Oxford University Press; 2007. p. 802
28. Wang, L. Photoacoustic Tomography -- Ultrasonically Beating Optical Diffusion and Diffraction. 2014. Available from: http://spie.org/x106504.xml
29. Maiti S, Shear JB, Williams RM, Zipfel WR, Webb WW. Measuring serotonin distribution in live cells with three-photon excitation. Science. 1997; 275(5299):530–2. [PubMed: 8999797]
30. Diaspro, A. Confocal and two-photon microscopy : foundations, applications, and advances. Vol. xix. New York: Wiley-Liss; 2002. p. 5674 p. of plates
31. Xu X, Liu H, Wang LV. Time-reversed ultrasonically encoded optical focusing into scattering media. Nature Photonics. 2011; 5(3):154. [PubMed: 21532925]
32. Wang YM, Judkewitz B, Dimarzio CA, Yang C. Deep-tissue focal fluorescence imaging with digitally time-reversed ultrasound-encoded light. Nat Commun. 2012; 3:928. [PubMed: 22735456]
33. Raju BI, Srinivasan MA. High-frequency ultrasonic attenuation and backscatter coefficients of in vivo normal human dermis and subcutaneous fat. Ultrasound in Medicine and Biology. 2001; 27(11):1543–1556. [PubMed: 11750754]
34. Azhari, H. Basics of biomedical ultrasound for engineers. Vol. xiii. Hoboken, N.J: Wiley : IEEE; 2010. p. 3712 p. of plates
35. Moran CM, Bush NL, Bamber JC. Ultrasonic propagation properties of excised human skin. Ultrasound in medicine & biology. 1995; 21(9):1177–90. [PubMed: 8849832]
36. Kessler LW. VHF ultrasonic attenuation in mammalian tissue. The Journal of the Acoustical Society of America. 1973; 53(6):1759–60. [PubMed: 4719261]
37. Zackrisson S, van de Ven SM, Gambhir SS. Light in and sound out: emerging translational strategies for photoacoustic imaging. Cancer Res. 2014; 74(4):979–1004. [PubMed: 24514041]
38. Kim C, Favazza C, Wang LHV. In Vivo Photoacoustic Tomography of Chemicals: High-Resolution Functional and Molecular Optical Imaging at New Depths. Chemical Reviews. 2010; 110(5):2756–2782. [PubMed: 20210338]
39. Ntziachristos V, Razansky D. Molecular Imaging by Means of Multispectral Optoacoustic Tomography (MSOT). Chemical Reviews. 2010; 110(5):2783–2794. [PubMed: 20387910]
40. Zhang HF, Maslov K, Li ML, Stoica G, Wang LHV. In vivo volumetric imaging of subcutaneous microvasculature by photoacoustic microscopy. Optics Express. 2006; 14(20):9317–9323. [PubMed: 19529315]
41. Zhou Y, Yi X, Xing W, Hu S, Maslov KI, Wang LV. Microcirculatory changes identified by photoacoustic microscopy in patients with complex regional pain syndrome type I after stellate ganglion blocks. Journal of Biomedical Optics. 2014; 19(8):086017. [PubMed: 25144451]

42. Song KH, Wang LV. Deep reflection-mode photoacoustic imaging of biological tissue. Journal of Biomedical Optics. 2007; 12(6):060503. [PubMed: 18163798]
43. Jeon M, Kim J, Kim C. Multiplane spectroscopic whole-body photoacoustic imaging of small animals in vivo. Medical & Biological Engineering & Computing. 2014:1–12.
44. Esenaliev RO, Karabutov AA, Oraevsky AA. Sensitivity of laser optoacoustic imaging in detection of small deeply embedded tumors. Ieee Journal of Selected Topics in Quantum Electronics. 1999; 5(4):981–988.
45. Manohar S, Vaartjes SE, van Hespen JCG, Klaase JM, van den Engh FM, Steenbergen W, et al. Initial results of in vivo non-invasive cancer imaging in the human breast using near-infrared photoacoustics. Optics Express. 2007; 15(19):12277–12285. [PubMed: 19547596]
46. Ermilov SA, Khamapirad T, Conjusteau A, Leonard MH, Lacewell R, Mehta K, et al. Laser optoacoustic imaging system for detection of breast cancer. Journal of Biomedical Optics. 2009; 14(2):024007. [PubMed: 19405737]
47. Kumon RE, Deng CX, Wang X. Frequency-domain analysis of photoacoustic imaging data from prostate adenocarcinoma tumors in a murine model. Ultrasound Med Biol. 2011; 37(5):834–839. [PubMed: 21376447]
48. Yaseen MA, Ermilov SA, Brecht HP, Su R, Conjusteau A, Fronheiser M, et al. Optoacoustic imaging of the prostate: development toward image-guided biopsy. Journal of Biomedical Optics. 2010; 15(2):021310. [PubMed: 20459232]
49. Silverman RH, Kong F, Chen YC, Lloyd HO, Kim HH, Cannata JM, et al. High-resolution photoacoustic imaging of ocular tissues. Ultrasound Med Biol. 2010; 36(5):733–742. [PubMed: 20420969]
50. Yang JM, Favazza C, Chen RM, Yao JJ, Cai X, Maslov K, et al. Simultaneous functional photoacoustic and ultrasonic endoscopy of internal organs in vivo. Nature Medicine. 2012; 18(8): 1297.
51. Xia J, Chatni MR, Maslov K, Guo Z, Wang K, Anastasio M, et al. Whole-body ring-shaped confocal photoacoustic computed tomography of small animals in vivo. Journal of Biomedical Optics. 2012; 17(5):050506. [PubMed: 22612121]
52. Gateau J, Caballero MA, Dima A, Ntziachristos V. Three-dimensional optoacoustic tomography using a conventional ultrasound linear detector array: whole-body tomographic system for small animals. Medical Physics. 2013; 40(1):013302. [PubMed: 23298121]
53. Brecht HP, Su R, Fronheiser M, Ermilov SA, Conjusteau A, Oraevsky AA. Whole-body three-dimensional optoacoustic tomography system for small animals. Journal of Biomedical Optics. 2009; 14(6):064007. [PubMed: 20059245]
54. Levi J, Kothapalli SR, Bohndiek S, Yoon JK, Dragulescu-Andrasi A, Nielsen C, et al. Molecular Photoacoustic Imaging of Follicular Thyroid Carcinoma. Clinical Cancer Research. 2013; 19(6): 1494–1502. [PubMed: 23349314]
55. Pramanik M, Ku G, Li C, Wang LV. Design and evaluation of a novel breast cancer detection system combining both thermoacoustic (TA) and photoacoustic (PA) tomography. Medical Physics. 2008; 35(6):2218–2223. [PubMed: 18649451]
56. Strohm EM, Berndl ES, Kolios MC. High frequency label-free photoacoustic microscopy of single cells. Photoacoustics. 2013; 1(3–4):49–53. [PubMed: 25302149]
57. Strohm EM, Berndl ESL, Kolios MC. Probing Red Blood Cell Morphology Using High-Frequency Photoacoustics. Biophysical Journal. 2013; 105(1):59–67. [PubMed: 23823224]
58. Cai X, Li L, Krumholz A, Guo ZJ, Erpelding TN, Zhang C, et al. Multi-Scale Molecular Photoacoustic Tomography of Gene Expression. Plos One. 2012; 7(8):e43999. [PubMed: 22952846]
59. Hu, S.; Gonzales, E.; Soetikno, B.; Gong, E.; Yan, P.; Maslov, K., et al. Photons Plus Ultrasound: Imaging and Sensing 2011. San Francisco, California, USA: SPIE; 2011. Optical-resolution photoacoustic microscopy of ischemic stroke; p. 789906–789906-5.
60. Hu S, Maslov K, Tsytsarev V, Wang LV. Functional transcranial brain imaging by optical-resolution photoacoustic microscopy. Journal of Biomedical Optics. 2009; 14(4):040503. [PubMed: 19725708]

61. Hu S, Maslov K, Wang LV. Second-generation optical-resolution photoacoustic microscopy with improved sensitivity and speed. Optics Letters. 2011; 36(7):1134–1136. [PubMed: 21479007]
62. Ku G, Maslov K, Li L, Wang LHV. Photoacoustic microscopy with 2-mu m transverse resolution. Journal of Biomedical Optics. 2010; 15(2):021302. [PubMed: 20459224]
63. Liu YY, Yang XQ, Gong H, Jiang BW, Wang H, Xu GQ, et al. Assessing the effects of norepinephrine on single cerebral microvessels using optical-resolution photoacoustic microscope. Journal of Biomedical Optics. 2013; 18(7):076007.
64. Maslov K, Zhang HF, Hu S, Wang LV. Optical-resolution photoacoustic microscopy for in vivo imaging of single capillaries. Optics Letters. 2008; 33(9):929–931. [PubMed: 18451942]
65. Rao B, Maslov K, Danielli A, Chen R, Shung KK, Zhou Q, et al. Real-time four-dimensional optical-resolution photoacoustic microscopy with Au nanoparticle-assisted subdiffraction-limit resolution. Optics Letters. 2011; 36(7):1137–9. [PubMed: 21479008]
66. Tsytsarev V, Hu S, Yao JJ, Maslov K, Barbour DL, Wang LV. Photoacoustic microscopy of microvascular responses to cortical electrical stimulation. Journal of Biomedical Optics. 2011; 16(7):076002. [PubMed: 21806263]
67. Wang H, Yang XQ, Liu YY, Jiang BW, Luo QM. Reflection-mode optical-resolution photoacoustic microscopy based on a reflective objective. Optics Express. 2013; 21(20):24210–24218. [PubMed: 24104331]
68. Wang LD, Maslov K, Yao JJ, Rao B, Wang LHV. Fast voice-coil scanning optical-resolution photoacoustic microscopy. Optics Letters. 2011; 36(2):139–141. [PubMed: 21263479]
69. Xia J, Li G, Wang LD, Nasiriavanaki M, Maslov K, Engelbach JA, et al. Wide-field two-dimensional multifocal optical-resolution photoacoustic-computed microscopy. Optics Letters. 2013; 38(24):5236–5239. [PubMed: 24322226]
70. Xie ZX, Jiao SL, Zhang HF, Puliafito CA. Laser-scanning optical-resolution photoacoustic microscopy. Optics Letters. 2009; 34(12):1771–1773. [PubMed: 19529698]
71. Xing WX, Wang LD, Maslov K, Wang LHV. Integrated optical- and acoustic-resolution photoacoustic microscopy based on an optical fiber bundle. Optics Letters. 2013; 38(1):52–54. [PubMed: 23282835]
72. Yao JJ, Huang CH, Wang LD, Yang JM, Gao L, Maslov KI, et al. Wide-field fast-scanning photoacoustic microscopy based on a water-immersible MEMS scanning mirror. Journal of Biomedical Optics. 2012; 17(8):080505. [PubMed: 23224156]
73. Estrada H, Turner J, Kneipp M, Razansky D. Real-time optoacoustic brain microscopy with hybrid optical and acoustic resolution. Laser Physics Letters. 2014; 11(4):045601.
74. Ma R, Sontges S, Shoham S, Ntziachristos V, Razansky D. Fast scanning coaxial optoacoustic microscopy. Biomedical Optics Express. 2012; 3(7):1724–1731. [PubMed: 22808441]
75. Zhang C, Maslov K, Wang LHV. Subwavelength-resolution label-free photoacoustic microscopy of optical absorption in vivo. Optics Letters. 2010; 35(19):3195–3197. [PubMed: 20890331]
76. Li G, Maslov KI, Wang LV. Reflection-mode multifocal optical-resolution photoacoustic microscopy. Journal of Biomedical Optics. 2013; 18(3):030501. [PubMed: 23446704]
77. Song LA, Maslov K, Wang LV. Multifocal optical-resolution photoacoustic microscopy in vivo. Optics Letters. 2011; 36(7):1236–1238. [PubMed: 21479041]
78. Langer G, Bouchal KD, Grun H, Burgholzer P, Berer T. Two-photon absorption-induced photoacoustic imaging of Rhodamine B dyed polyethylene spheres using a femtosecond laser. Optics Express. 2013; 21(19):22410–22. [PubMed: 24104130]
79. Yamaoka Y, Nambu M, Takamatsu T. Fine depth resolution of two-photon absorption-induced photoacoustic microscopy using low-frequency bandpass filtering. Optics Express. 2011; 19(14): 13365–77. [PubMed: 21747492]
80. Urban BE, Yi J, Yakovlev V, Zhang HF. Investigating femtosecond-laser-induced two-photon photoacoustic generation. Journal of Biomedical Optics. 2014; 19(8):085001. [PubMed: 25084119]
81. Yao JJ, Wang LD, Li CY, Zhang C, Wang LHV. Photoimprint Photoacoustic Microscopy for Three-Dimensional Label-Free Subdiffraction Imaging. Physical Review Letters. 2014; 112(1): 014302. [PubMed: 24483902]

82. Danielli A, Maslov K, Garcia-Uribe A, Winkler AM, Li C, Wang L, et al. Label-free photoacoustic nanoscopy. Journal of Biomedical Optics. 2014; 19(8):086006. [PubMed: 25104412]
83. Nedosekin DA, Galanzha EI, Dervishi E, Biris AS, Zharov VP. Super-Resolution Nonlinear Photothermal Microscopy. Small. 2013:135–142. [PubMed: 23864531]
84. Deng ZL, Wang Z, Yang XQ, Luo QM, Gong H. In vivo imaging of hemodynamics and oxygen metabolism in acute focal cerebral ischemic rats with laser speckle imaging and functional photoacoustic microscopy. Journal of Biomedical Optics. 2012; 17(8):081415. [PubMed: 23224176]
85. Burton NC, Patel M, Morscher S, Driessen WHP, Claussen J, Beziere N, et al. Multispectral Opto-acoustic Tomography (MSOT) of the Brain and Glioblastoma Characterization. Neuroimage. 2013; 65:522–528. [PubMed: 23026761]
86. Liao LD, Lin CT, Shih YYI, Duong TQ, Lai HY, Wang PH, et al. Transcranial imaging of functional cerebral hemodynamic changes in single blood vessels using in vivo photoacoustic microscopy. Journal of Cerebral Blood Flow and Metabolism. 2012; 32(6):938–951. [PubMed: 22472612]
87. Zhang HF, Maslov K, Sivaramakrishnan M, Stoica G, Wang LHV. Imaging of hemoglobin oxygen saturation variations in single vessels in vivo using photoacoustic microscopy. Applied Physics Letters. 2007; 90(5):053901.
88. Danielli A, Favazza CP, Maslov K, Wang LHV. Single-wavelength functional photoacoustic microscopy in biological tissue. Optics Letters. 2011; 36(5):769–771. [PubMed: 21368977]
89. Guo ZJ, Hu S, Wang LHV. Calibration-free absolute quantification of optical absorption coefficients using acoustic spectra in 3D photoacoustic microscopy of biological tissue. Optics Letters. 2010; 35(12):2067–2069. [PubMed: 20548388]
90. Jo J, Yang X. Functional photoacoustic imaging to observe regional brain activation induced by cocaine hydrochloride. Journal of Biomedical Optics. 2011; 16(9):090506. [PubMed: 21950909]
91. Sivaramakrishnan M, Maslov K, Zhang HF, Stoica G, Wang LV. Limitations of quantitative photoacoustic measurements of blood oxygenation in small vessels. Physics in Medicine and Biology. 2007; 52(5):1349–1361. [PubMed: 17301459]
92. Yang XM, Stein EW, Ashkenazi S, Wang LHV. Nanoparticles for photoacoustic imaging. Wiley Interdisciplinary Reviews-Nanomedicine and Nanobiotechnology. 2009; 1(4):360–368. [PubMed: 20049803]
93. Pramanik M, Wang LV. Thermoacoustic and photoacoustic sensing of temperature. Journal of Biomedical Optics. 2009; 14(5):054024. [PubMed: 19895126]
94. Winkler AM, Maslov K, Wang LV. Noise-equivalent sensitivity of photoacoustics. Journal of Biomedical Optics. 2013; 18(9):097003. [PubMed: 24026425]
95. Wang LD, Xia J, Yao JJ, Maslov KI, Wang LHV. Ultrasonically Encoded Photoacoustic Flowgraphy in Biological Tissue. Physical Review Letters. 2013; 111(20):204301. [PubMed: 24289689]
96. Bauer AQ, Nothdurft RE, Erpelding TN, Wang LHV, Culver JP. Quantitative photoacoustic imaging: correcting for heterogeneous light fluence distributions using diffuse optical tomography. Journal of Biomedical Optics. 2011; 16(9):096016. [PubMed: 21950930]
97. Brunker, J.; Beard, P. Photons Plus Ultrasound: Imaging and Sensing 2010. San Francisco, California, USA: SPIE; 2010. Pulsed photoacoustic Doppler flowmetry using a cross correlation method; p. 756426-8.
98. Chen SL, Ling T, Huang SW, Won Baac H, Guo LJ. Photoacoustic correlation spectroscopy and its application to low-speed flow measurement. Optics Letters. 2010; 35(8):1200–1202. [PubMed: 20410966]
99. Fang H, Maslov K, Wang LV. Photoacoustic Doppler effect from flowing small light-absorbing particles. Physical Review Letters. 2007; 99(18):184501. [PubMed: 17995411]
100. Sheinfeld A, Eyal A. Photoacoustic thermal diffusion flowmetry. Biomedical Optics Express. 2012; 3(4):800–813. [PubMed: 22574267]
101. Wang L, Yao J, Maslov KI, Xing W, Wang LV. Ultrasound-heated photoacoustic flowmetry. Journal of Biomedical Optics. 2013; 18(11):117003. [PubMed: 24194064]

102. Yao JJ, Wang LHV. Transverse flow imaging based on photoacoustic Doppler bandwidth broadening. Journal of Biomedical Optics. 2010; 15(2):021304. [PubMed: 20459226]
103. Chatni MR, Yao JJ, Danielli A, Favazza CP, Maslov KI, Wang LHV. Functional photoacoustic microscopy of pH. Journal of Biomedical Optics. 2011; 16(10):100503. [PubMed: 22029342]
104. Duan ZY, Gao YJ, Qiao ZY, Fan G, Liu Y, Zhang D, et al. A photoacoustic approach for monitoring the drug release of pH-sensitive poly(beta-amino ester)s. Journal of Materials Chemistry B. 2014; 2(37):6271–6282.
105. Huang GJ, Si Z, Yang SH, Li C, Xing D. Dextran based pH-sensitive near-infrared nanoprobe for in vivo differential-absorption dual-wavelength photoacoustic imaging of tumors. Journal of Materials Chemistry. 2012; 22(42):22575–22581.
106. Horvath TD, Kim G, Kopelman R, Ashkenazi S. Ratiometric photoacoustic sensing of pH using a “sonophore”. Analyst. 2008; 133(6):747–749. [PubMed: 18493674]
107. MacKenzie HA, Ashton HS, Spiers S, Shen YC, Freeborn SS, Hannigan J, et al. Advances in photoacoustic noninvasive glucose testing. Clinical Chemistry. 1999; 45(9):1587–1595. [PubMed: 10471673]
108. Yeh C, Hu S, Maslov K, Wang LV. Photoacoustic microscopy of blood pulse wave. Journal of Biomedical Optics. 2012; 17(7):070504. [PubMed: 22894460]
109. Song W, Wei Q, Liu WZ, Liu T, Yi J, Sheibani N, et al. A combined method to quantify the retinal metabolic rate of oxygen using photoacoustic ophthalmoscopy and optical coherence tomography. Scientific Reports. 2014; 4:6525. [PubMed: 25283870]
110. Liu T, Wei Q, Wang J, Jiao SL, Zhang HF. Combined photoacoustic microscopy and optical coherence tomography can measure metabolic rate of oxygen. Biomedical Optics Express. 2011; 2(5):1359–1365. [PubMed: 21559147]
111. Hsia CC. Respiratory function of hemoglobin. The New England journal of medicine. 1998; 338(4):239–247. [PubMed: 9435331]
112. Cox B, Laufer JG, Arridge SR, Beard PC. Quantitative spectroscopic photoacoustic imaging: a review. Journal of Biomedical Optics. 2012; 17(6):061202. [PubMed: 22734732]
113. Luis Dean-Ben X, Razansky D. Adding fifth dimension to optoacoustic imaging: volumetric time-resolved spectrally enriched tomography. Light Sci Appl. 2014; 3:e137.
114. Maslov K, Zhang HF, Wang LV. Effects of wavelength-dependent fluence attenuation on the noninvasive photoacoustic imaging of hemoglobin oxygen saturation in subcutaneous vasculature in vivo. Inverse Problems. 2007; 23(6):S113–S122.
115. Wang J, Liu T, Jiao SL, Chen RM, Zhou QF, Shung KK, et al. Saturation effect in functional photoacoustic imaging. Journal of Biomedical Optics. 2010; 15(2):021317. [PubMed: 20459239]
116. Xie ZX, Wang LHV, Zhang HF. Optical fluence distribution study in tissue in dark-field confocal photoacoustic microscopy using a modified Monte Carlo convolution method. Applied Optics. 2009; 48(17):3204–3211. [PubMed: 19516366]
117. Xia J, Danielli A, Liu Y, Wang L, Maslov K, Wang LV. Calibration-free quantification of absolute oxygen saturation based on the dynamics of photoacoustic signals. Optics Letters. 2013; 38(15):2800–3. [PubMed: 23903146]
118. Shao Q, Morgounova E, Jiang C, Choi J, Bischof J, Ashkenazi S. In vivo photoacoustic lifetime imaging of tumor hypoxia in small animals. Journal of Biomedical Optics. 2013; 18(7):076019. [PubMed: 23877772]
119. Mallidi S, Luke GP, Emelianov S. Photoacoustic imaging in cancer detection, diagnosis, and treatment guidance. Trends Biotechnol. 2011; 29(5):213–221. [PubMed: 21324541]
120. Schule G, Huttmann G, Framme C, Roider O, Brinkmann R. Noninvasive optoacoustic temperature determination at the fundus of the eye during laser irradiation. Journal of Biomedical Optics. 2004; 9(1):173–179. [PubMed: 14715070]
121. Larina IV, Larin KV, Esenaliev RO. Real-time optoacoustic monitoring of temperature in tissues. Journal of Physics D-Applied Physics. 2005; 38(15):2633–2639.
122. Kandulla J, Elsner H, Birngruber R, Brinkmann R. Noninvasive optoacoustic online retinal temperature determination during continuous-wave laser irradiation. Journal of Biomedical Optics. 2006; 11(4):041111. [PubMed: 16965139]

123. Nikitin SM, Khokhlova TD, Pelivanov IM. Temperature dependence of the optoacoustic transformation efficiency in ex vivo tissues for application in monitoring thermal therapies. Journal of Biomedical Optics. 2012; 17(6):061214. [PubMed: 22734744]

124. Petrova E, Ermilov S, Su R, Nadvoretskiy V, Conjusteau A, Oraevsky A. Using optoacoustic imaging for measuring the temperature dependence of Gruneisen parameter in optically absorbing solutions. Optics Express. 2013; 21(21):25077–25090. [PubMed: 24150350]

125. Petrova EV, Oraevsky AA, Ermilov SA. Red blood cell as a universal optoacoustic sensor for non-invasive temperature monitoring. Applied Physics Letters. 2014; 105(9):094103. [PubMed: 25316928]

126. Serebryakov VA, Boiko EV, Yan AV. Real-time optoacoustic monitoring of the temperature of the retina during laser therapy. Journal of Optical Technology. 2014; 81(6):312–321.

127. Rao KS, Yehya F, Chaudhary AK, Kumar AS, Sahoo AK. Thermal stability study of nitro-rich triazole derivatives using temperature dependent time resolved pulsed photoacoustic (PA) technique. Journal of Analytical and Applied Pyrolysis. 2014; 109:132–139.

128. Shah J, Park S, Aglyamov S, Larson T, Ma L, Sokolov K, et al. Photoacoustic imaging and temperature measurement for photothermal cancer therapy. Journal of Biomedical Optics. 2008; 13(3):034024. [PubMed: 18601569]

129. Yao J, Wang LV. Photoacoustic microscopy. Laser & Photonics Reviews. 2013; 7(5):758–778.

130. Yao L, Huang H, Jiang H. Finite-element-based photoacoustic imaging of absolute temperature in tissue. Optics Letters. 2014; 39(18):5355–5358. [PubMed: 26466270]

131. Zhang R, Wang L, Yao J, Yeh CH, Wang LV. In vivo optically encoded photoacoustic flowgraphy. Optics Letters. 2014; 39(13):3814–3817. [PubMed: 24978744]

132. Fang H, Maslov K, Wang LV. Photoacoustic Doppler flow measurement in optically scattering media. Applied Physics Letters. 2007; 91(26):264103.

133. Sheinfeld, A.; Gilead, S.; Eyal, A. Photons Plus Ultrasound: Imaging and Sensing 2010. San Francisco, California, USA: SPIE; 2010. Time-resolved photoacoustic Doppler characterization of flow using pulsed excitation; p. 75643N-6

134. Yao J, Maslov KI, Shi Y, Taber LA, Wang LV. In vivo photoacoustic imaging of transverse blood flow by using Doppler broadening of bandwidth. Optics Letters. 2010; 35(9):1419–1221. [PubMed: 20436589]

135. Yao JJ, Gilson RC, Maslov KI, Wang LD, Wang LHV. Calibration-free structured-illumination photoacoustic flowgraphy of transverse flow in scattering media. Journal of Biomedical Optics. 2014; 19(4):046007. [PubMed: 24718385]

136. Zhang RY, Yao JJ, Maslov KI, Wang LHV. Structured-illumination photoacoustic Doppler flowmetry of axial flow in homogeneous scattering media. Applied Physics Letters. 2013; 103(9):094101.

137. Zhang RY, Wang LD, Yao JJ, Yeh CH, Wang LHV. In vivo optically encoded photoacoustic flowgraphy. Optics Letters. 2014; 39(13):3814–3817. [PubMed: 24978744]

138. Razansky D, Buehler A, Ntziachristos V. Volumetric real-time multispectral optoacoustic tomography of biomarkers. Nature Protocols. 2011; 6(8):1121–1129. [PubMed: 21738125]

139. Razansky D, Distel M, Vinegoni C, Ma R, Perrimon N, Koster RW, et al. Multispectral opto-acoustic tomography of deep-seated fluorescent proteins in vivo. Nature Photonics. 2009; 3(7): 412–417.

140. Razansky D, Vinegoni C, Ntziachristos V. Multispectral photoacoustic imaging of fluorochromes in small animals. Optics Letters. 2007; 32(19):2891–2893. [PubMed: 17909608]

141. de la Zerda A, Kim JW, Galanzha EI, Gambhir SS, Zharov VP. Advanced contrast nanoagents for photoacoustic molecular imaging, cytometry, blood test and photothermal theranostics. Contrast Media & Molecular Imaging. 2011; 6(5):346–369. [PubMed: 22025336]

142. Galanzha EI, Shashkov EV, Kelly T, Kim JW, Yang LL, Zharov VP. In vivo magnetic enrichment and multiplex photoacoustic detection of circulating tumour cells. Nature Nanotechnology. 2009; 4(12):855–860.

143. Taruttis A, Herzog E, Razansky D, Ntziachristos V. Real-time imaging of cardiovascular dynamics and circulating gold nanorods with multispectral optoacoustic tomography. Optics Express. 2010; 18(19):19592–19602. [PubMed: 20940855]

144. Wang YW, Xie XY, Wang XD, Ku G, Gill KL, O'Neal DP, et al. Photoacoustic tomography of a nanoshell contrast agent in the in vivo rat brain. Nano Letters. 2004; 4(9):1689–1692.

145. Su R, Ermilov SA, Liopo AV, Oraevsky AA. Three-dimensional optoacoustic imaging as a new noninvasive technique to study long-term biodistribution of optical contrast agents in small animal models. Journal of Biomedical Optics. 2012; 17(10):101506. [PubMed: 23223982]

146. Tsyboulski DA, Liopo AV, Su R, Ermilov SA, Bachilo SM, Weisman RB, et al. Enabling in vivo measurements of nanoparticle concentrations with three-dimensional optoacoustic tomography. Journal of Biophotonics. 2014; 7(8):581–8. [PubMed: 23554158]

147. Yao J, Wang LV. Sensitivity of photoacoustic microscopy. Photoacoustics. 2014; 2(2):87–101. [PubMed: 25302158]

148. Bouchard LS, Anwar MS, Liu GL, Hann B, Xie ZH, Gray JW, et al. Picomolar sensitivity MRI and photoacoustic imaging of cobalt nanoparticles. Proceedings of the National Academy of Sciences of the United States of America. 2009; 106(11):4085–4089. [PubMed: 19251659]

149. de la Zerda A, Liu ZA, Bodapati S, Teed R, Vaithilingam S, Khuri-Yakub BT, et al. Ultrahigh Sensitivity Carbon Nanotube Agents for Photoacoustic Molecular Imaging in Living Mice. Nano Letters. 2010; 10(6):2168–2172. [PubMed: 20499887]

150. Oraevsky, AA.; Karabutov, AA. Biomedical Optoacoustics. San Jose, CA: SPIE; 2000. Ultimate sensitivity of time-resolved optoacoustic detection; p. 228-239.

151. Razansky D, Baeten J, Ntziachristos V. Sensitivity of molecular target detection by multispectral optoacoustic tomography (MSOT). Medical Physics. 2009; 36(3):939–945. [PubMed: 19378754]

152. Eghtedari M, Oraevsky A, Copland JA, Kotov NA, Conjusteau A, Motamedi M. High sensitivity of in vivo detection of gold nanorods using a laser optoacoustic imaging system. Nano Letters. 2007; 7(7):1914–8. [PubMed: 17570730]

153. Copland JA, Eghtedari M, Popov VL, Kotov N, Mamedova N, Motamedi M, et al. Bioconjugated gold nanoparticles as a molecular based contrast agent: implications for imaging of deep tumors using optoacoustic tomography. Molecular imaging and biology : MIB : the official publication of the Academy of Molecular Imaging. 2004; 6(5):341–9. [PubMed: 15380744]

154. Chatni MR, Xia J, Sohn R, Maslov K, Guo ZJ, Zhang Y, et al. Tumor glucose metabolism imaged in vivo in small animals with whole-body photoacoustic computed tomography. Journal of Biomedical Optics. 2012; 17(7):076012. [PubMed: 22894495]

155. Yao J, Xia J, Maslov KI, Nasiriavanaki M, Tsytsarev V, Demchenko AV, et al. Noninvasive photoacoustic computed tomography of mouse brain metabolism in vivo. Neuroimage. 2013; 64:257–66. [PubMed: 22940116]

156. Galanzha EI, Nedosekin DA, Sarimollaoglu M, Orza AI, Biris AS, Verkhusha VV, et al. Photoacoustic and photothermal cytometry using photoswitchable proteins and nanoparticles with ultrasharp resonances. Journal of Biophotonics. 2013 Eearly publication.

157. Wang Y, Maslov K, Zhang Y, Hu S, Yang LM, Xia YN, et al. Fiber-laser-based photoacoustic microscopy and melanoma cell detection. Journal of Biomedical Optics. 2011; 16(1):011014. [PubMed: 21280901]

158. Bhattacharyya K, Goldschmidt BS, Hannink M, Alexander S, Jurkevic A, Viator JA. Gold Nanoparticle-Mediated Detection of Circulating Cancer Cells. Clinics in Laboratory Medicine. 2012; 32(1):89. [PubMed: 22340845]

159. Juratli MA, Sarimollaoglu M, Siegel ER, Nedosekin DA, Galanzha EI, Suen JY, et al. Real-time monitoring of circulating tumor cell release during tumor manipulation using in vivo photoacoustic and fluorescent flow cytometry. Head and Neck-Journal for the Sciences and Specialties of the Head and Neck. 2014; 36(8):1207–1215.

160. Tzoumas S, Nunes A, Deliolanis NC, Ntziachristos V. Effects of multispectral excitation on the sensitivity of molecular optoacoustic imaging. J Biophotonics. 2014; 9999(9999)

161. Dean-Ben XL, Bay E, Razansky D. Functional optoacoustic imaging of moving objects using microsecond-delay acquisition of multispectral three-dimensional tomographic data. Scientific Reports. 2014; 4:5878. [PubMed: 25073504]

162. Dean-Ben XL, Razansky D. Adding fifth dimension to optoacoustic imaging: volumetric time-resolved spectrally enriched tomography. Light-Science & Applications. 2014; 3

163. Wang Y, Maslov K, Wang LHV. Spectrally encoded photoacoustic microscopy using a digital mirror device. Journal of Biomedical Optics. 2012; 17(6):066020. [PubMed: 22734776]

164. Wang L, Maslov K, Wang LV. Single-cell label-free photoacoustic flowoxigraphy in vivo. Proceedings of the National Academy of Sciences of the United States of America. 2013; 110(15):5759–64. [PubMed: 23536296]

165. Bauer AQ, Nothdurft RE, Erpelding TN, Wang LV, Culver JP. Quantitative photoacoustic imaging: correcting for heterogeneous light fluence distributions using diffuse optical tomography. Journal of Biomedical Optics. 2011; 16(9):096016. [PubMed: 21950930]

166. Li XQ, Xi L, Jiang RX, Yao L, Jiang HB. Integrated diffuse optical tomography and photoacoustic tomography: phantom validations. Biomedical Optics Express. 2011; 2(8):2348–2353. [PubMed: 21833371]

167. Xiaoqi L, Huabei J. Impact of inhomogeneous optical scattering coefficient distribution on recovery of optical absorption coefficient maps using tomographic photoacoustic data. Physics in Medicine and Biology. 2013; 58(4):999. [PubMed: 23339968]

168. Xu C, Kumavor PD, Alqasemi U, Li H, Xu Y, Zanganeh S, et al. Indocyanine green enhanced co-registered diffuse optical tomography and photoacoustic tomography. Journal of Biomedical Optics. 2013; 18(12):126006–126006. [PubMed: 24343437]

169. Yin L, Wang Q, Zhang Q, Jiang H. Tomographic imaging of absolute optical absorption coefficient in turbid media using combined photoacoustic and diffusing light measurements. Optics Letters. 2007; 32(17):2556–8. [PubMed: 17767303]

170. Xia J, Huang C, Maslov K, Anastasio MA, Wang LV. Enhancement of photoacoustic tomography by ultrasonic computed tomography based on optical excitation of elements of a full-ring transducer array. Opt Lett. 2013; 38(16):3140–3143. [PubMed: 24104670]

171. Treeby BE. Acoustic attenuation compensation in photoacoustic tomography using time-variant filtering. Journal of Biomedical Optics. 2013; 18(3):036008–036008. [PubMed: 23503580]

172. Dean-Ben XL, Razansky D, Ntziachristos V. The effects of acoustic attenuation in optoacoustic signals. Physics in Medicine and Biology. 2011; 56(18):6129–48. [PubMed: 21873768]

173. Dean-Ben XL, Ntziachristos V, Razansky D. Artefact reduction in optoacoustic tomographic imaging by estimating the distribution of acoustic scatterers. Journal of Biomedical Optics. 2012; 17(11):110504. [PubMed: 23096956]

174. Li L, Maslov K, Ku G, Wang LV. Three-dimensional combined photoacoustic and optical coherence microscopy for in vivo microcirculation studies. Optics Express. 2009; 17(19):16450–16455. [PubMed: 19770860]

175. Qin C, Cheng K, Chen K, Hu X, Liu Y, Lan X, et al. Tyrosinase as a multifunctional reporter gene for Photoacoustic/MRI/PET triple modality molecular imaging. Sci Rep. 2013; 3

176. Kircher MF, de la Zerda A, Jokerst JV, Zavaleta CL, Kempen PJ, Mittra E, et al. A brain tumor molecular imaging strategy using a new triple-modality MRI-photoacoustic-Raman nanoparticle. Nature Medicine. 2012; 18(5):829–834.

177. Akers WJ, Edwards WB, Kim C, Xu BG, Erpelding TN, Wang LHV, et al. Multimodal sentinel lymph node mapping with single-photon emission computed tomography (SPECT)/computed tomography (CT) and photoacoustic tomography. Translational Research. 2012; 159(3):175–181. [PubMed: 22340767]

178. Wang Y, Hu S, Maslov K, Zhang Y, Xia YN, Wang LV. In vivo integrated photoacoustic and confocal microscopy of hemoglobin oxygen saturation and oxygen partial pressure. Optics Letters. 2011; 36(7):1029–1031. [PubMed: 21478972]

179. Abran M, Cloutier G, Cardinal MH, Chayer B, Tardif JC, Lesage F. Development of a photoacoustic, ultrasound and fluorescence imaging catheter for the study of atherosclerotic plaque. IEEE Trans Biomed Circuits Syst. 2014; 8(5):696–703. [PubMed: 25350946]

180. Jiao SL, Jiang MS, Hu JM, Fawzi A, Zhou QF, Shung KK, et al. Photoacoustic ophthalmoscopy for in vivo retinal imaging. Optics Express. 2010; 18(4):3967–3972. [PubMed: 20389409]

181. Song W, Wei Q, Liu T, Kuai D, Burke JM, Jiao S, et al. Integrating photoacoustic ophthalmoscopy with scanning laser ophthalmoscopy, optical coherence tomography, and fluorescein angiography for a multimodal retinal imaging platform. Journal of Biomedical Optics. 2012; 17(6):061206–7. [PubMed: 22734736]

182. Tsytsarev V, Rao B, Maslov KI, Li L, Wang LHV. Photoacoustic and optical coherence tomography of epilepsy with high temporal and spatial resolution and dual optical contrasts. Journal of Neuroscience Methods. 2013; 216(2):142–145. [PubMed: 23603664]

183. Lee C, Han S, Kim S, Jeon M, Jeon MY, Kim C, et al. Combined photoacoustic and optical coherence tomography using a single near-infrared supercontinuum laser source. Applied Optics. 2013; 52(9):1824–1828. [PubMed: 23518723]

184. Gateau J, Caballero MAA, Dima A, Ntziachristos V. Three-dimensional optoacoustic tomography using a conventional ultrasound linear detector array: Whole-body tomographic system for small animals. Medical Physics. 2013; 40(1):013302. [PubMed: 23298121]

185. Wilson KE, Wang TY, Willmann JK. Acoustic and Photoacoustic Molecular Imaging of Cancer. Journal of Nuclear Medicine. 2013; 54(11):1851–1854. [PubMed: 24187042]

186. Harrison T, Ranasinghesagara JC, Lu HH, Mathewson K, Walsh A, Zemp RJ. Combined photoacoustic and ultrasound biomicroscopy. Optics Express. 2009; 17(24):22041–22046. [PubMed: 19997449]

187. Rao B, Soto F, Kerschensteiner D, Wang LV. Integrated photoacoustic, confocal, and two-photon microscope. Journal of Biomedical Optics. 2014; 19(3):36002. [PubMed: 24589986]

188. Lai P, Wang L, Tay JW, Wang L. Nonlinear photoacoustic wavefront shaping (PAWS) for single speckle-grain optical focusing in scattering media. Nature Photonics. 2015 in press.

189. Conkey, Donald B.; Caravaca-Aguirre, Antonio M.; Dove, Jacob D.; Ju, Hengyi; Murray, Todd W.; Piestun, R. Super-resolution photoacoustic imaging through a scattering wall. 2013. arXiv1310.5736

190. Li H, Dong BQ, Zhang Z, Zhang HF, Sun C. A transparent broadband ultrasonic detector based on an optical micro-ring resonator for photoacoustic microscopy. Scientific Reports. 2014; 4:4496. [PubMed: 24675547]

191. Zhang, EZ.; Beard, PC. SPIE BiOS. International Society for Optics and Photonics; 2011. A miniature all-optical photoacoustic imaging probe; p. 78991F–78991F-6.

192. Chen SL, Xie ZX, Ling T, Guo LJ, Wei XB, Wang XD. Miniaturized all-optical photoacoustic microscopy based on microelectromechanical systems mirror scanning. Optics Letters. 2012; 37(20):4263–4265. [PubMed: 23073431]

193. Miida, Y.; Matsuura, Y. SPIE BiOS. International Society for Optics and Photonics; 2014. Optical-fiber based all-optical 3D photoacoustic imaging system; p. 894331–894331-7.

194. Bell, MAL.; Guo, X.; Song, DY.; Boctor, EM. SPIE BiOS. International Society for Optics and Photonics; 2014. Photoacoustic imaging of prostate brachytherapy seeds with transurethral light delivery; p. 89430N–89430N-6.

195. Viator JA, Au G, Paltauf G, Jacques SL, Prahl SA, Ren HW, et al. Clinical testing of a photoacoustic probe for port wine stain depth determination. Lasers in Surgery and Medicine. 2002; 30(2):141–148. [PubMed: 11870794]

196. Yuan KH, Yuan Y, Gu Y, Gao JH, Xing D. In vivo photoacoustic imaging of model of port wine stains. Journal of X-Ray Science and Technology. 2012; 20(2):249–254. [PubMed: 22635179]

197. Brecht HP, Prough DS, Petrov YY, Patrikeev I, Petrova IY, Deyo DJ, et al. In vivo monitoring of blood oxygenation in large veins with a triple-wavelength optoacoustic system. Optics Express. 2007; 15(24):16261–16269. [PubMed: 19550914]

198. Kim C, Erpelding TN, Maslov K, Jankovic L, Akers WJ, Song LA, et al. Handheld array-based photoacoustic probe for guiding needle biopsy of sentinel lymph nodes. Journal of Biomedical Optics. 2010; 15(4):046010. [PubMed: 20799812]

199. Dean-Ben XL, Razansky D. Functional optoacoustic human angiography with handheld video rate three dimensional scanner. Photoacoustics. 2013; 1(3–4):68–73. [PubMed: 25302151]

200. Zhou Y, Xing WX, Maslov KI, Cornelius LA, Wang LHV. Handheld photoacoustic microscopy to detect melanoma depth in vivo. Optics Letters. 2014; 39(16):4731–4734. [PubMed: 25121860]

201. Adachi Y, Hoshimiya T. Photoacoustic Imaging with Multiple-Wavelength Light-Emitting Diodes. Japanese Journal of Applied Physics. 2013; 52(7):07HB06.

202. Bell, MAL.; Guo, X.; Kang, HJ.; Boctor, E. Ultrasonics Symposium (IUS), 2014 IEEE International. IEEE; 2014. Improved contrast in laser-diode-based photoacoustic images with short-lag spatial coherence beamforming; p. 37-40.

203. Zeng LM, Liu GD, Yang DW, Ji XR. 3D-visual laser-diode-based photoacoustic imaging. Optics Express. 2012; 20(2):1237–1246. [PubMed: 22274468]

204. Kolkman RGM, Steenbergen W, van Leeuwen TG. In vivo photoacoustic imaging of blood vessels with a pulsed laser diode. Lasers in Medical Science. 2006; 21(3):134–139. [PubMed: 16721626]

205. Li, M-L.; Wang, P-H. SPIE BiOS. International Society for Optics and Photonics; 2014. Optical resolution photoacoustic microscopy using a Blu-ray DVD pickup head; p. 894315–894315-6.

206. Yapici MK, Kim C, Chang CC, Jeon M, Guo ZJ, Cai X, et al. Parallel acoustic delay lines for photoacoustic tomography. Journal of Biomedical Optics. 2012; 17(11):116019. [PubMed: 23139043]

207. Cho Y, Chang CC, Yu J, Jeon M, Kim C, Wang LV, et al. Handheld photoacoustic tomography probe built using optical-fiber parallel acoustic delay lines. Journal of Biomedical Optics. 2014; 19(8):086007. [PubMed: 25104413]

208. Danielli A, Maslov K, Garcia-Uribe A, Winkler AM, Li CY, Wang LD, et al. Label-free photoacoustic nanoscopy. Journal of Biomedical Optics. 2014; 19(8):086006. [PubMed: 25104412]

209. Kircher MF, de la Zerda A, Jokerst JV, Zavaleta CL, Kempen PJ, Mittra E, et al. A brain tumor molecular imaging strategy using a new triple-modality MRI-photoacoustic-Raman nanoparticle. Nature Medicine. 2012; 18(5):829–U235.

210. Laufer, J.; Jathoul, A.; Johnson, P.; Zhang, E.; Lythgoe, M.; Pedley, RB., et al. Photons Plus Ultrasound: Imaging and Sensing 2012. San Francisco, California, USA: SPIE; 2012. In vivo photoacoustic imaging of tyrosinase expressing tumours in mice; p. 82230M-5

211. Pu KY, Shuhendler AJ, Jokerst JV, Mei JG, Gambhir SS, Bao ZN, et al. Semiconducting polymer nanoparticles as photoacoustic molecular imaging probes in living mice. Nature Nanotechnology. 2014; 9(3):233–239.

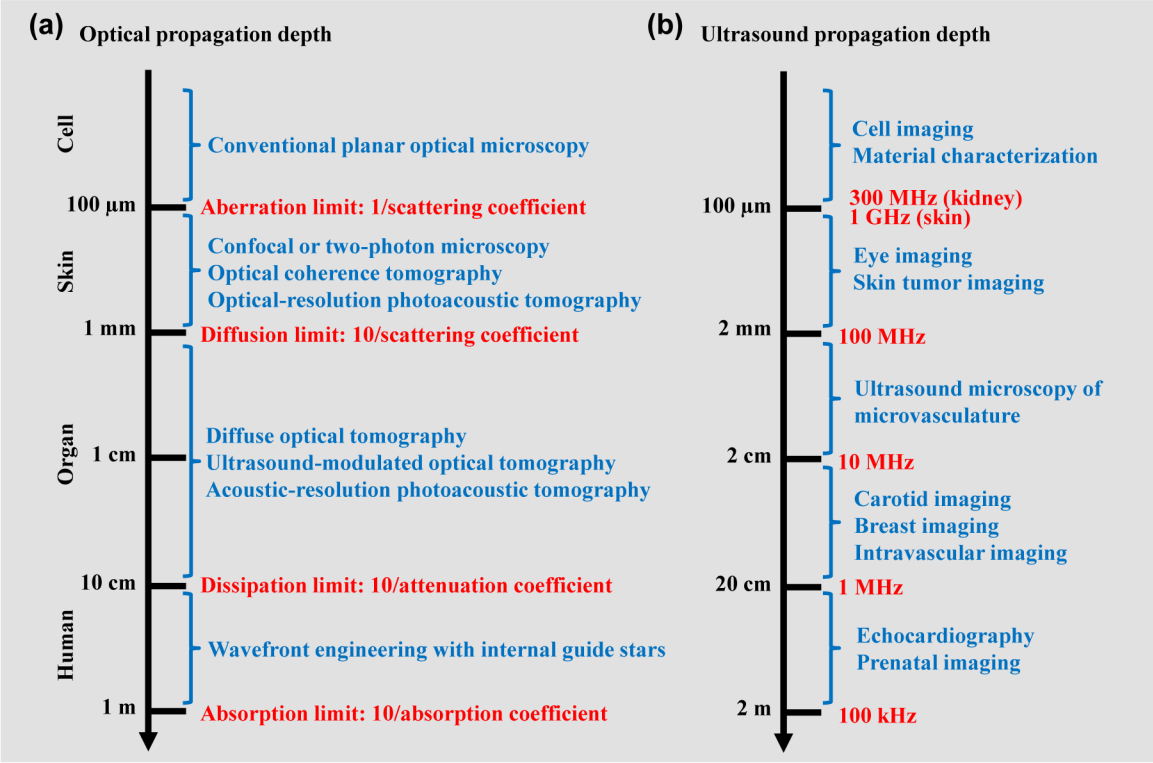

Figure 1. Photon and ultrasound propagation regimes in soft tissue

(a) Photon propagation regimes in soft tissue, which are approximately related to the penetration depths of representative optical imaging modalities [5, 28]. The four regimes are divided at photon propagation depths of 0.1 mm, 1 mm, 10 cm and 1 m, with typical optical absorption coefficient of 0.1 cm^{-1}, optical scattering coefficient of 100 cm^{-1} and anisotropy of 0.9. The classification holds in optical scattering dominant media. (b) Ultrasound propagation regimes at typical ultrasound frequencies in soft tissue, with corresponding biomedical applications [34]. The ultrasound attenuation coefficient is approximately proportional to the ultrasound frequency up to at least 300 MHz for skin [35] and 100 MHz for kidney [36]. Here, the −10 dB propagation depth at the frequency up to 100 MHz is estimated with an ultrasound attenuation coefficient of 0.5 dB/cm/MHz. The propagation depths at 300 MHz for kidney and 1 GHz for skin are extrapolated based on the literature data [35, 36], taking into account the ultrasound attenuation by water.

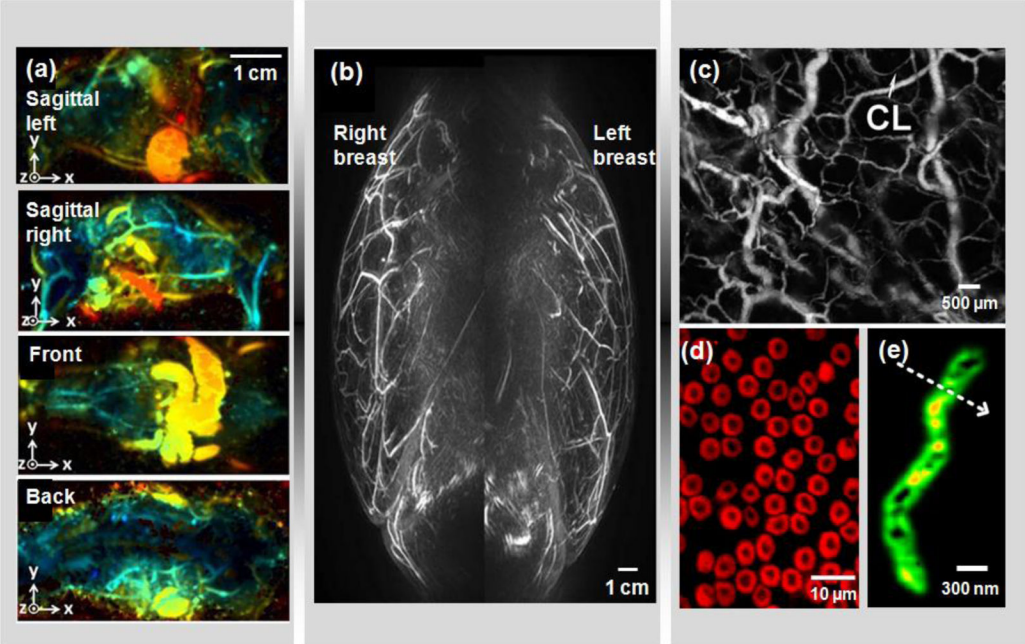

Figure 2. Multi-scale PAT

(a) Whole-body PAT of a mouse *in vivo* [43]. Acquired at 1064 nm, the maximum amplitude projection (MAP) images were extracted from sagittal, front and back views. The depths are color encoded from blue (shallow) to red (deep). (b) Medial-lateral MAP image of breasts of a healthy volunteer [12]. A semi-spherical transducer array was used with rotational scanning. (c) Optical-resolution photoacoustic microscopy (OR-PAM) of mouse ear vasculature, where single capillaries (CL) can be clearly resolved [64]. (d) Sub-wavelength OR-PAM of single red blood cells [75]. A lateral resolution of ~220 nm was achieved. (e) Photoacoustic nanoscopy of a mitochondrion in a fibroblast cell [208]. A lateral resolution of ~80 nm was achieved by using the optical absorption saturation effect. Images were adapted with permission from references [12, 43, 64, 75, 208].

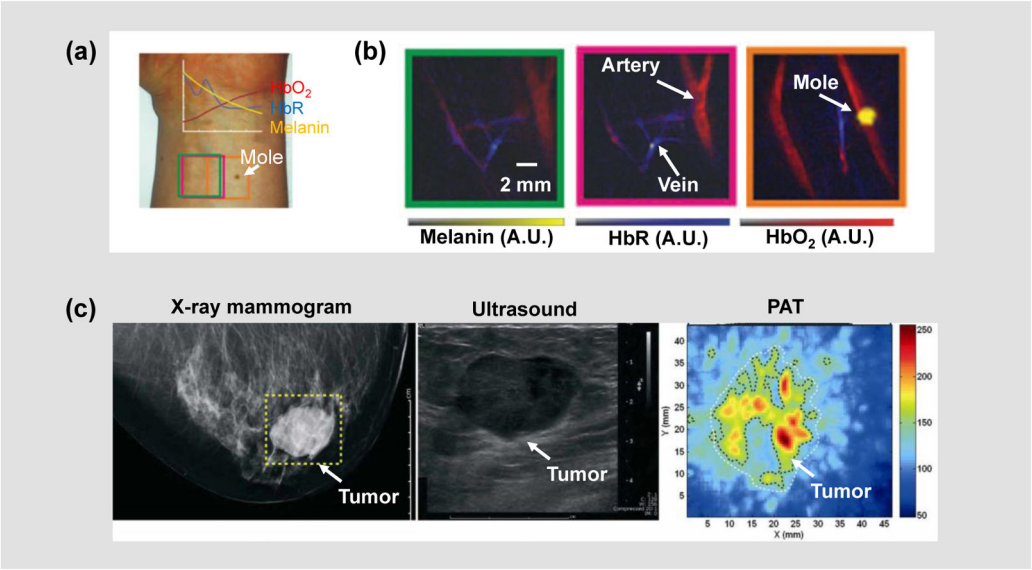

Figure 3. Functional PAT

(a) A photograph of a healthy volunteer's forearm, from which hand-held PACT images were taken [162]. The colored boxes correspond to the regions of interest imaged by PACT. HbR, deoxy-hemoglobin; HbO_2, oxy-hemoglobin. (b) Spectrally unmixed PA oxygenation images of the three boxed regions shown in (a). (c) PAT of an invasive ductal carcinoma in the right breast of a 57-year-old woman [45]. Left to right: X-ray mammogram (left); ultrasound image (middle); and PAT image (right). The higher PA signal strength in the PAT image was attributed to tumor angiogenesis. Images were adapted with permission from references [45, 162].

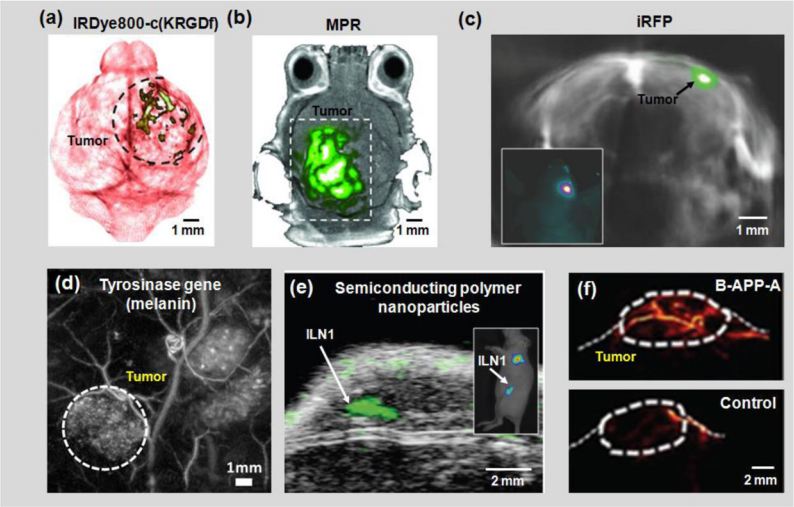

Figure 4. Molecular PAT

(a) PAT of a glioblastoma in a mouse brain enhanced by IRDye800-c(KRGDf), which targeted overexpressed integrin $\alpha_{v\beta3}$ in tumor cells [7]. (b) PAT of a glioblastoma in a mouse brain enhanced by tri-modality MRI-PA-Raman (MPR) nanoparticles [209]. (c) PAT of an iRFP-expressing glioblastoma in a mouse brain, 25 days post implantation [160]. The spectrally unmixed signals from the tumor (shown in green) are superimposed on the signals from blood (shown in gray). iRFP, infrared fluorescent protein. Inset: epi-fluorescence image of the mouse brain showing the tumor location. (d) PAT of a subcutaneous tyrosinase-expressing tumor [210]. The tumor is marked by the dashed circle. (e) Ultrasound (shown in gray) and photoacoustic (shown in green) co-registered image of mouse lymph nodes following tail vein injection of semiconducting polymer nanoparticles (SPN) [211]. ILN, inguinal lymph node. Inset: epi-fluorescence image of the mouse showing the ILN location. (f) PAT of the activatable B-APP-A in a FTC133 tumor in the mouse hind leg after tail vein injection of B-APP-A (top) and the control probe (bottom) [54]. Images were adapted with permission from references [7, 54, 160, 209–211].

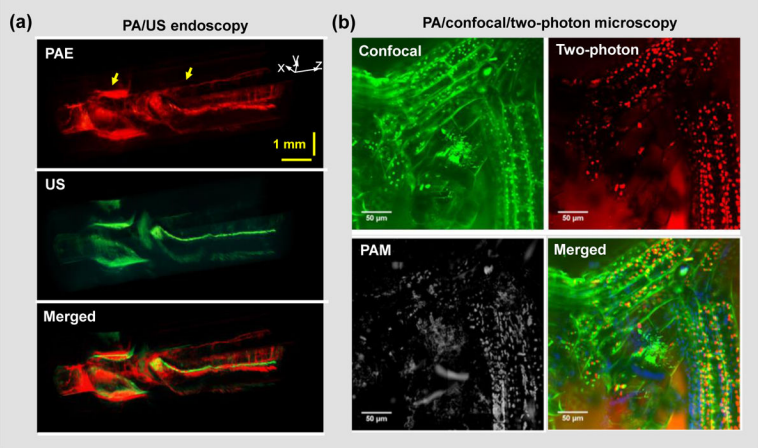

Figure 5. Integration of PAT with other imaging modalities

(a) Integrated PA/ultrasound (US) endoscopy of the upper esophagus of a rabbit *in vivo* [50]. The PA and US imaging share the same ultrasound transducer and scanning system. (b) Integrated PA/confocal/two-photon microscopy of a moss leaf [187]. The three imaging modalities share the same optical paths and scanning system. Images were adapted with permission from references [50, 187].